PAPER • OPEN ACCESS

Thermoplastic 3D printing technology using a single filament for producing realistic patient-derived breast models

To cite this article: Nikolay Dukov *et al* 2022 *Phys. Med. Biol.* **67** 045008

Physics in Medicine & Biology

IPEM Institute of Physics and Engineering in Medicine

PAPER

Thermoplastic 3D printing technology using a single filament for producing realistic patient-derived breast models

Nikolay Dukov[1], **Kristina Bliznakova**[1], **Nikiforos Okkalidis**[2], **Tsvetelina Teneva**[3], **Elitsa Encheva**[3] and **Zhivko Bliznakov**[1]

[1] Department of Medical Equipment, Electronic and Information Technologies in Healthcare, Medical University of Varna, Varna, Bulgaria
[2] Morphé, Thessaloniki, Greece
[3] Department of Imaging Diagnostics, Interventional Radiology and Radiotherapy, Medical University of Varna, Bulgaria

E-mail: kristina.bliznakova@mu-varna.bg **and** kristina.bliznakova@gmail.com

Keywords: physical breast phantoms, 3D printing, fused-deposition modelling, PLA filament, MRI breast, CT breast, segmentation algorithm

OPEN ACCESS

RECEIVED
6 July 2021

REVISED
22 December 2021

ACCEPTED FOR PUBLICATION
17 January 2022

PUBLISHED
10 February 2022

Abstract

Objective. This work describes an approach for producing physical anthropomorphic breast phantoms from clinical patient data using three-dimensional (3D) fused-deposition modelling (FDM) printing. *Approach*. The source of the anthropomorphic model was a clinical Magnetic Resonance Imaging (MRI) patient image set, which was segmented slice by slice into adipose and glandular tissues, skin and tumour formations; thus obtaining a four component computational breast model. The segmented tissues were mapped to specific Hounsfield Units (HU) values, which were derived from clinical breast Computed Tomography (CT) data. The obtained computational model was used as a template for producing a physical anthropomorphic breast phantom using 3D printing. FDM technology with only one polylactic acid filament was used. The physical breast phantom was scanned at Siemens SOMATOM Definition CT. Quantitative and qualitative evaluation were carried out to assess the clinical realism of CT slices of the physical breast phantom. *Main results*. The comparison between selected slices from the computational breast phantom and CT slices of the physical breast phantom shows similar visual x-ray appearance of the four breast tissue structures: adipose, glandular, tumour and skin. The results from the task-based evaluation, which involved three radiologists, showed a high degree of realistic clinical radiological appearance of the modelled breast components. Measured HU values of the printed structures are within the range of HU values used in the computational phantom. Moreover, measured physical parameters of the breast phantom, such as weight and linear dimensions, agreed very well with the corresponding ones of the computational breast model. *Significance*. The presented approach, based on a single FDM material, was found suitable for manufacturing of a physical breast phantom, which mimics well the 3D spatial distribution of the different breast tissues and their x-ray absorption properties. As such, it could be successfully exploited in advanced x-ray breast imaging research applications.

1. Introduction

Anthropomorphic phantoms are both computational and physical models of the human body, organs, tissues or part of it, and they are considered an excellent tool for comparison, characterization and optimization of existing diagnostic modalities. In the field of breast imaging, anthropomorphic breast models are used for an assessment of the diagnostic task performance of breast imaging systems without conducting long and high cost clinical trials (Ikejimba *et al* 2018), optimizing clinical protocols, image processing and reconstruction algorithms (Bliznakova *et al* 2010, Malliori *et al* 2012, Malliori *et al* 2014), as well as for research on new breast imaging systems and their technical optimization (Mettivier *et al* 2017, Glick and Ikejimba, 2018, Bliznakova, 2020).

Recent studies demonstrated their main role in 'virtual clinical trials', which aim to replace the randomized control clinical trials, thus reducing the time and expenses related processes, as well as administering of additional radiation dose to patients. Attempts to create anthropomorphic breast phantoms dates with the advent of 3D medical imaging modalities, while the development of the 3D printing technologies have accelerated their manufacturing, when used for specific imaging tasks (Bliznakova, 2020). In this respect, two approaches have gained popularity: (a) based on 2D mammography images and (b) based on 3D computational breast models. Schopphoven *et al* (Schopphoven *et al* 2019) used a PolyJet 3D printer and a polypropylene like printing material Rigur RGD450™, to print a breast anthropomorphic phantom with printable structures with a size of about 200 μm. A similar approach for producing an anthropomorphic breast phantom was proposed by Badal *et al* (Badal *et al* 2018). The key element in the methodology of these two groups is the calculation of the x-ray attenuation at each pixel position of the clinical mammographic image, and further this attenuation is simulated by the differences in the height of the printing material, resulting in a relief-like structure on top of the printed phantom. The obtained physical breast phantoms are explicitly dedicated for quality control activities, as well as for exploring new and optimising the existing clinical acquisition protocols for the current 2D mammography units.

There are two widely used methods for manufacturing of physical breast phantoms based on 3D computational breast models: (i) printing the different breast structures separately, followed by assembling the complete breast phantom as demonstrated by several investigators (Carton *et al* 2011, Kiarashi *et al* 2015, Dukov *et al* 2019, Dukov *et al* 2021), and (ii) printing the whole phantom 'at once' by using two (di Franco *et al* 2019) or a single printing material (Daskalov *et al* 2020). Most of these phantoms are limited to printing the glandular and the adipose tissues, which are the main breast tissues. Attempts to print breast phantoms with lesions were recently reported by few authors (Di Franco *et al* 2019, Dukov *et al* 2019, Dukov *et al* 2021), showing that suitable materials for printing breast abnormalities are still to be developed and investigated for x-ray applications (Ivanov *et al* 2018, Santos *et al* 2019). Much effort has been devoted to the development of new 3D printing materials like, photopolymers doped with different concentration of TiO_2, calcium, iodine and zinc (Sikaria *et al* 2016, Zhao *et al* 2017). A major challenge and a requirement in the field of x-ray breast imaging is the use of 3D printing materials with x-ray absorption characteristics close to these of the breast tissues, particularly for the energy range used in mammography.

The aim of this study is to demonstrate a new approach in developing of realistic in size and content three-dimensional physical breast models based on real patient MRI images. The novelty concerns the computational modelling of the anthropomorphic phantom and the use of one printing material to successfully simulate the x-ray attenuation of the four breast tissue types. The physical breast phantom is dedicated to current research in design and testing novel 3D imaging techniques.

2. Materials and methods

2.1. Overall approach

The overall methodology for the creation of both, the computational and the physical breast phantoms, is shown in figure 1.

Initially, a female breast is scanned at an MRI system equipped with a breast facility, which procedure resulted in several MRI breast image sets. Then, a selected MRI set is segmented slice by slice into adipose, glandular, skin and lesion tissues. The computational breast phantom is assembled from the four segmented tissue volumes, as the voxel values have been assigned Hounsfield Units (HUs) representing the specific breast tissue type. Its physical version is obtained via 3D printing technique. The appropriateness of this approach for obtaining physical anthropomorphic breast models is further assessed through a direct comparison between slices from the computational breast phantom and the CT breast volume of the scanned breast physical phantom at a CT facility. Finally, a detailed comparison of the physical parameters of the computational and physical breast phantoms, such as weight and linear dimensions, is accomplished.

2.2. Patient data

The breast model is based on a set of MRI images from a right breast of a 57-year-old patient diagnosed with invasive ductal carcinoma G2-3 Stage pT1b pNo Mo. The acquisition of the patients' MRI image sets was performed with GE Signa HDxt MRI scanner. In the current study the segmentation was realised on a T1-weigthed image set from the Axial multi-phase VIBRANT (3-phase) sequence, for which the voxel size is 0.7 mm $\times$ 0.7 mm $\times$ 0.8 mm. Contrast agent is used for the clinical procedure. This retrospective study was approved by the Ethics Committee of Medical University of Varna (Approval number 102/22.04.2021).

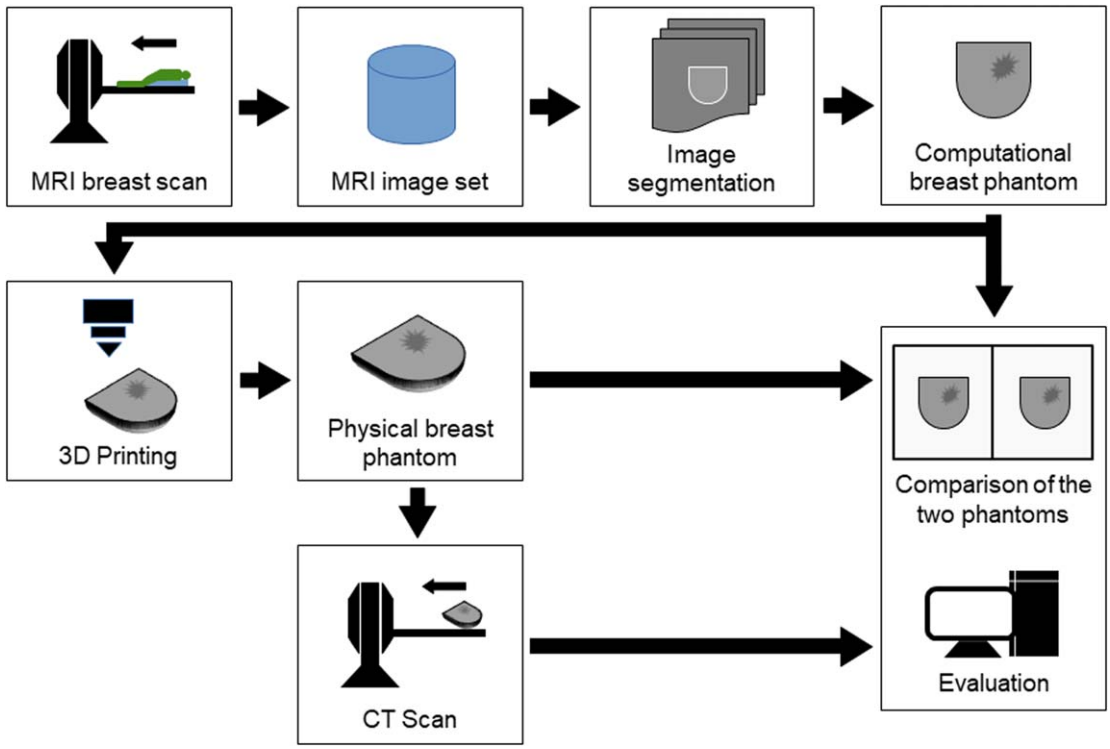

Figure 1. An overview of the approach for creating both, the computational and the physical breast phantoms.

2.3. Segmentation

The segmentation algorithm is based on our approach for segmenting breast lesions from clinical breast computed tomography and breast tomosynthesis data (Dukov *et al* 2019), that was modified for segmenting breast skin, adipose, glandular and lesion tissues. Figure 2 outlines the main steps in segmenting the breast MRI image set.

The obtained patient specific MRI image set is subjected to a semi-automatic segmentation applied for each breast tissue. The segmentation algorithm includes: (i) choosing the region of interest (ROI), then performing (ii) a threshold operation in order to separate the tissue of interest, followed by (iii) morphological operations, which reduce the artifacts, and finally (iv) a manual artifact reduction performed by an experienced radiologist to further minimize artifacts. The thresholding operation involves adjusting a single parameter for the different tissues (skin tissue, glandular tissue and lesion formation), which is done empirically. This is implemented based on the function *imbinarise* with the adaptive method in MATLAB 2020. The morphological operations involve 'area opening' on the resulting binary images, based on the *bwareaopen* function. The 'area opening' is performed in two dimensions for an eight-connected neighbourhood. The segmentation procedure is applied for each of the following tissues: (a) skin, (b) glandular, and (c) lesion formation.

The adipose tissue is obtained as following. First, the three segmented tissues (skin, glandular, lesion) are combined into one. Then a mask is generated with a size and shape similar to the segmented skin, but with infill, which results in a mask covering the whole breast. Afterwards, the adipose tissue is segmented based on the difference between the object created from the three segmented tissues and the created mask. Finally, all tissues (skin, glandular, lesion, and adipose) are added together, thus forming the complete computational breast model.

2.4. Computational phantom of the breast

The computational breast phantom includes a procedure that assigns unique values to the segmented breast tissues as specified in table 1. The density of the tissues was adopted from Berger *et al* (Berger *et al* 2010) and Ivanov *et al* (Ivanov *et al* 2018), while the assigned HUs were measured from patients breast CT (Bliznakova *et al* 2019, Dukov *et al* 2019). For this purpose, three breast mastectomy specimens with lesions were scanned at Siemens SOMATOM Definition CT with 80 kVp, voxel size of 0.32 mm $\times$ 0.32 mm $\times$ 0.6 mm. Following breast removal surgery, the mastectomy specimens were placed in a sterilised plastic container and immediately scanned in a fresh condition. Regions with skin, adipose, glandular and tumour tissues were segmented in the CT slices with the assistance of radiologists. The measured HU values with the standard deviations are reported

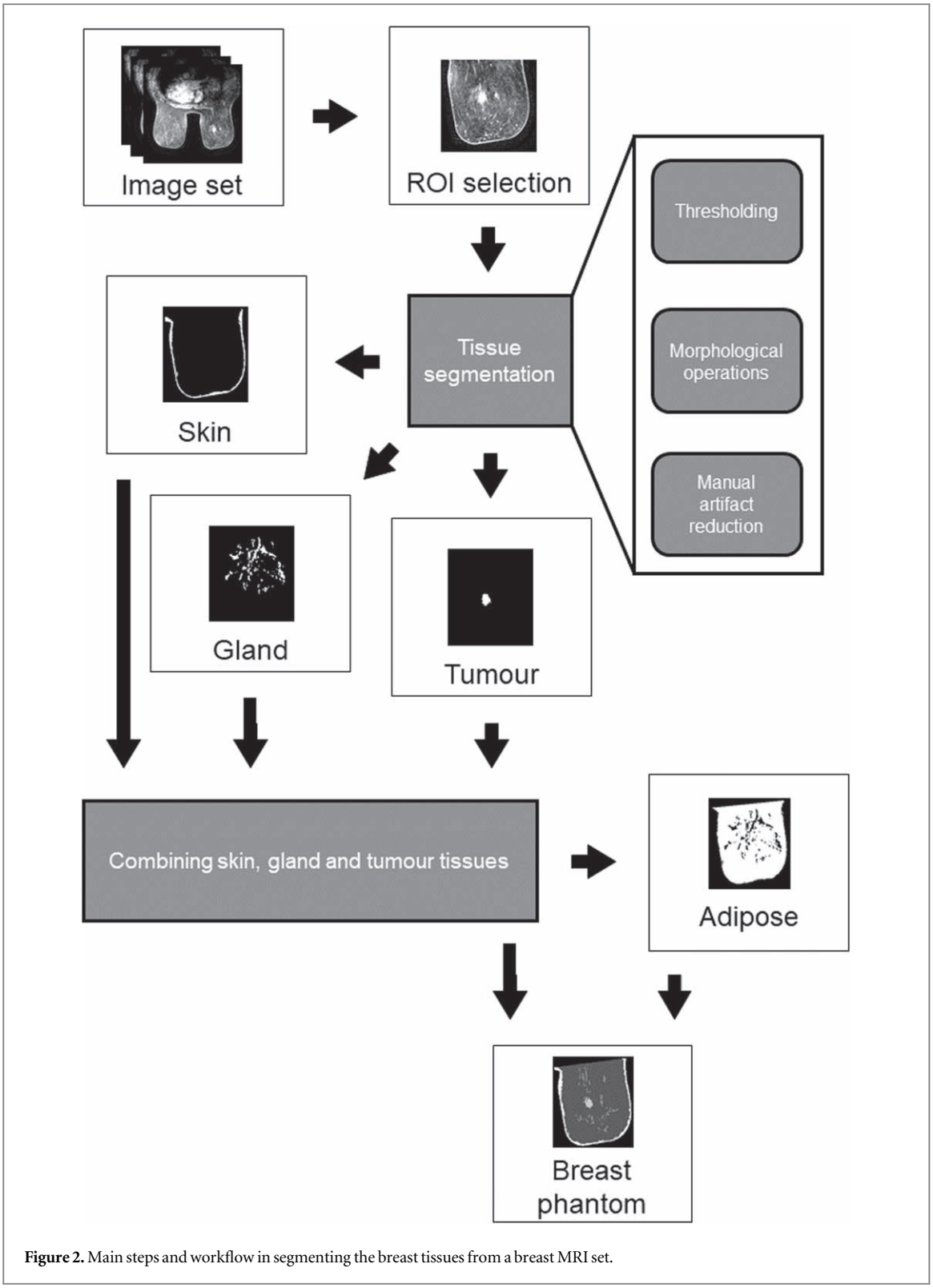

Figure 2. Main steps and workflow in segmenting the breast tissues from a breast MRI set.

Table 1. Assigned properties of the simulated breast tissues and values measured from CT scans of mastectomies.

Tissue/Material	Measured HUs and SD from CT scanned mastectomies	HUs chosen for the creation of the model	Density, g cm^{-3}
Skin	108 ± 21	108	1.09
Adipose tissue	−152 ± 15	−152	0.95
Glandular tissue	42 ± 11	42	1.04
Tumour	64 ± 17	64	1.05

in table 1. Based on the measured HU data for the different tissues, the average values for the HUs were selected to create the computational CT breast model.

2.5. Printing setup

In a previous work, it was demonstrated that it is possible a 3D printed patient-specific phantom to be fabricated by controlling the filament extrusion rate in correspondence with the HU retrieved from each voxel from a patient's CT scan DICOM image set (Okkalidis, 2018, Daskalov *et al* 2020). To achieve a realistic appearance from an MRI data set and a correspondence to CT, specific HUs were selected for each segmented entity. Thus, in this work we used two new approaches for the fabrication of a 3D printed anthropomorphic phantom based on an MRI data: (a) a constant filament extrusion rate for each voxel, which means a specific amount of melted filament has been extruded to each voxel belonging to a specific tissue and (b) a perimetric pattern for the replication of the small entities with more irregular shapes, such as the glandular and the tumour tissues. The perimetric pattern is available on a commercial software such as PrusaSlicer or Cura, however, in this study it was used accompanied by a filament extrusion method. A custom-made software written in MATLAB 2020 was used to control Multoo MT2-B 3D printer with a printing volume 500 mm × 500 mm × 600 mm. The extruder consists of a Volcano Hotend and a 0.4 mm nozzle. The polylactic acid (PLA) Easyfil PLA filament (Formfutura, Holland) with a density of1.24 g cm^{-3} and 1.75 mm diameter was the selected filament for the replication of the segmented tissues. The temperature of the extruder was set to 180 °C, and the bed was heated to 60 °C. The printing speed was constant at 30 mm s^{-1}, while the layer height was chosen at 0.25 mm. The literature review on FDM printing shows that polylactic acid (PLA) and acrylonitrile butadiene styrene (ABS) are the most common materials used for fabrication of phantoms dedicated to radiation therapy (Tino *et al* 2019). In this study, PLA was chosen because it can be printed without the warping effects that are common with ABS. The x-ray absorption characteristics of PLA were studied for the energies of the x-rays between 30 keV and 60 keV (Ivanov *et al* 2018), showing always higher attenuation in respect to breast tissues. However, reduced-density PLA turns out to match the x-ray properties of the breast tissues (Daskalov *et al* 2020).

The fabrication of the phantom requires the use of two 3D printing patterns: (a) a linear pattern, and (b) a perimetric pattern. The linear pattern is related to printing of the selected area line-by-line. The perimetric pattern relates to the identification and printing of an area's perimeter, and is followed by a new identification and printing of a new perimeter derived from the rest of the selected area. It is repeated until the whole area of the entity has been printed out. By employing the perimetric pattern compared to a linear pattern, a complex entity can be fully covered minimizing the travelling of the nozzle above the already printed entities and reducing the filament retractions, thus minimizing the negative effect the retractions may have on the replicated HUs. A calibration procedure was carried out for both 3D printing patterns, i.e. the linear and the perimetric, which includes 3D printing of four cubes with dimensions 20 mm × 20 mm × 20 mm under various filament extrusion rates (Okkalidis, 2018, Okkalidis and Marinakis, 2020). The cubes were CT scanned (figure 3(a)) and the retrieved HUs were correlated with the various filament extrusion rates, as shown in figure 3(b). HU values were measured on a ROI of size 10 mm × 10 mm. The equations, which define the lines fitted on measurements of the cubes (figure 3(b)), were used for the correlation of the extrusion rates with the corresponding HUs. A PLA filament can be used to replicate soft tissue with a range of −700 HU up to 150 HU, approximately (Okkalidis, 2018), and hence those two values were used during the 3D printing process as a lower- and an upper

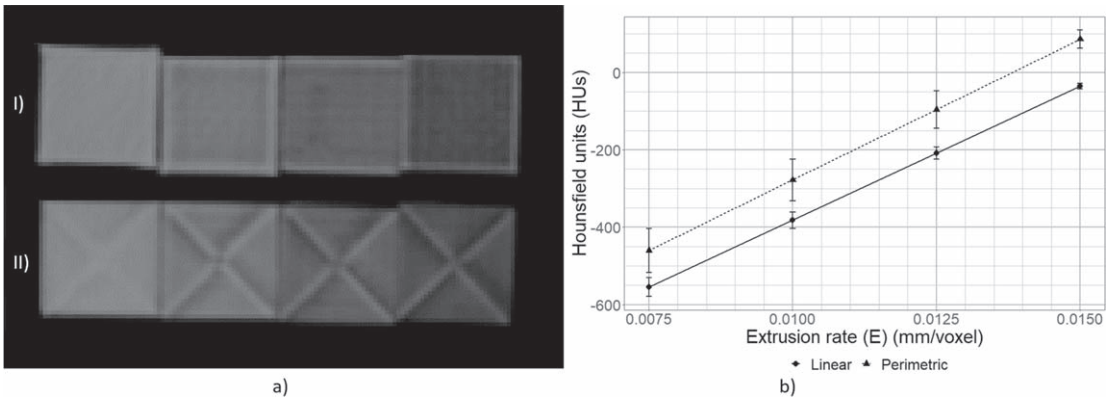

Figure 3. Calibration procedure: (a) an image from a CT scan of the two groups of cubes, 3D printed with (I) the linear and (II) the perimetric pattern; (b) a correlation of the extrusion rates with the HUs with standard deviation for the linear and the perimetric 3D printing patterns. The physical meaning of the extrusion rate (***E***) is the movement of the filament per voxel in mm.

Table 2. HU retrieved from the calibration cubes for the linear and perimetric 3D printing patterns.

Extrusion rate ($\boldsymbol{E}$) (mm voxel^{-1})	Mean HU and SD (Linear pattern)	Min/Max HU (Linear pattern)	Mean HU and SD (Perimetric pattern)	Min/Max HU (Perimetric pattern)
0.015	−35 ± 7	−108/+14	86 ± 23	−56/+142
0.0125	−208 ± 15	−375/−178	−96 ± 48	−236/+24
0.01	−381 ± 21	−449/−328	−278 ± 54	−389/−107
0.0075	−554 ± 24	−665/−501	−460 ± 57	−571/−273

cut-off values, respectively. The perimetric pattern compared to the linear pattern has demonstrated higher HUs for the same filament extrusion rates because it has accumulated small amounts of melted filament when there was a change in the printing direction (shown in table 2 and figure 3(b)). In figure 3(a), the first group of cubes (figures 3(a-I)) was printed using the linear pattern, while the second group of cubes (figure 3(a-II)) was printed with the perimetric pattern. In the same figure, the accumulated amounts of the filament due to the direction change are observable in the second group, where the perimetric pattern was used. This is the reason for the higher standard deviations noticed for the perimetric pattern compared to the standard deviations of the linear pattern. Furthermore, the standard deviations of both patterns were increasing as the extrusion rate was decreasing, due to the less melted filament was deposited per voxel and the larger air gaps in the printed cubes.

The complete phantom was printed as follows: the glandular and the tumour tissues were printed by using the perimetric pattern, while the skin and the adipose tissues were printed together using the linear pattern. The selected HUs for the adipose, glandular, tumour and skin were −152, 42, 64 and 108, respectively. Four extrusion rates were selected using the curves and the above selected HUs shown in figure 3(b). Furthermore, an edge detection algorithm was applied to detect the boundaries between the skin and adipose tissue, and the retrieved boundaries were printed with the extrusion filament rate used for adipose tissue, thus, outlining the difference between the printed adipose and skin tissues. The calibration cubes and the physical breast phantom were scanned at Siemens SOMATOM Definition CT, 80 kVp, 39 mAs. The voxel size of the scanned volume was 0.96 mm × 0.96 mm × 3 mm.

2.6. Evaluation

Subjective and objective approaches were used to carry out a preliminary evaluation of the proposed methodology for 3D physical breast modelling. A task-based evaluation was designed for the physical breast phantom. The study involved three radiologists with more than 10 years of experience in the field of radiology and a specifically defined questionnaire with selected CT slices from the scanned physical breast model. The design of this study was influenced by the design of similar studies addressing the modelling of irregular masses (Bliznakova *et al* 2003, Elangovan *et al* 2018), where researchers used in-house Java-based plug-in (Image 1.5i) and power point presentation for assessing the realism of simulated breast masses. The main questions are summarized in table 3, and were formulated to depict various scenarios for assessment, where the different structures in the breast phantom were or were not observable.

In all cases, the radiologists were able to adjust the contrast of the evaluated images, displayed on a clinical monitor EIZO RadiForce MX242W. The radiologists were not familiar with the clinical MRI scan before evaluating the phantom images. For the purposes of this evaluation, five image sets (each one containing a pair of images) were prepared. Image set 1 contained two consecutive CT axial slices from the scanned physical breast volume. Image set 2 also contained two consecutive CT axial slices from the scanned physical breast volume, different from image set 1. Image sets 3 and 4 were similar to image sets 1 and 2, however they contained CT coronal slices from the scanned physical breast volume. Finally, image set 5 consisted of one CT slice from the scanned physical breast phantom and the corresponding slice from the computational breast model.

The questionnaire was composed of five sections, related to each image set. Each section used the same set of questions, listed in table 3, applied to each image set.

Table 3. Questions used in the questionnaire for the evaluation of the physical breast phantom.

Questions
Is there any lesion in the images?
Is the lesion realistic?
What is the type of the lesion?
Do you distinguish the individual breast tissues (glandular tissue, adipose tissue, lesions, and skin) from the model?
Are the modelled breast components realistic?
Is the breast model realistic as a whole?

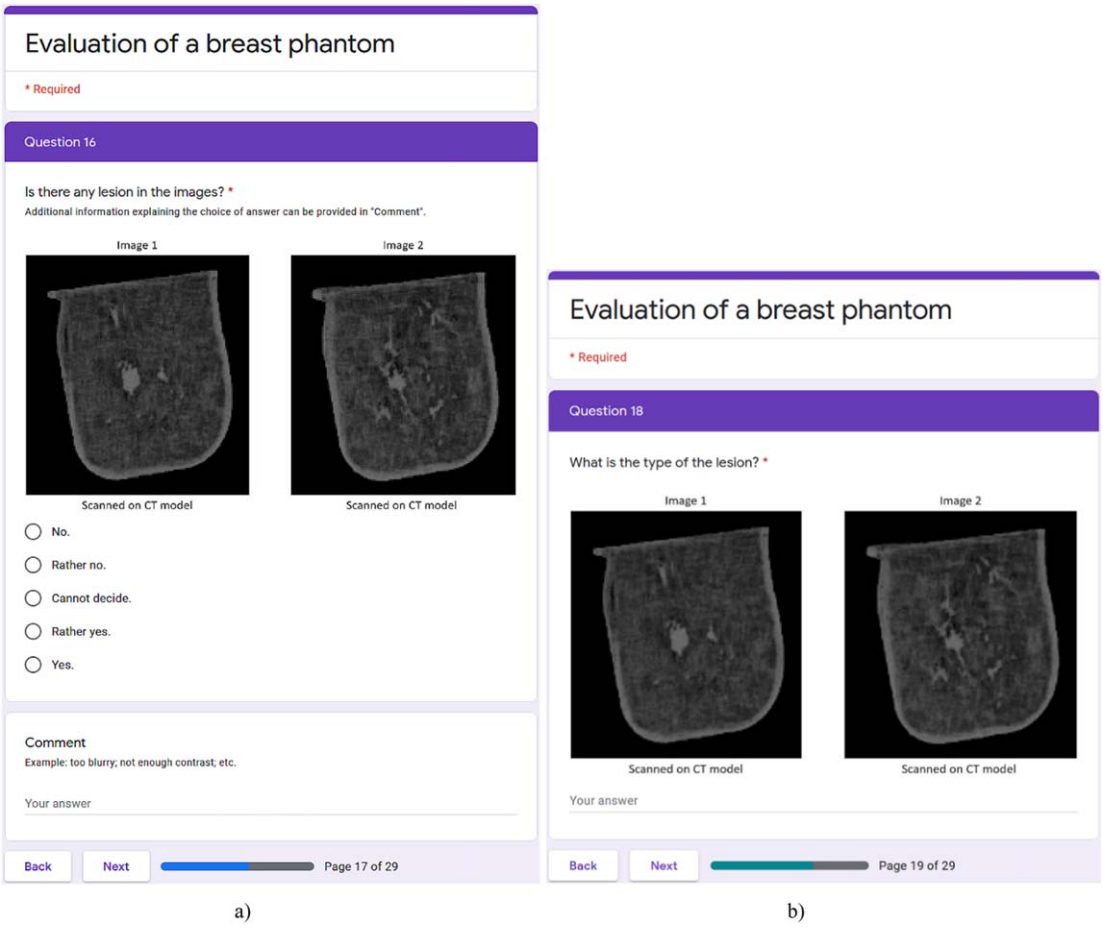

Figure 4. Screenshots of two questions of the evaluation study: (a) a multiple choice question with an optional comment section, (b) a question with a free plain text answer.

The answers to the questions were limited to multiple choice, with the option to select only one answer. There were five options for the answers—(1) No; (2) Rather no; (3) Cannot decide; (4) Rather yes; (5) Yes as shown in figure 4(a). In addition, there was a comment box, in which the evaluator could provide additional comments in regards to his/her answer. An exception was the free plain text question 'What is the type of the lesion?', shown in figure 4(b). There was no restriction on the viewing time during the assessment. The objective evaluation included measurements of the physical parameters of the model, profile comparison, and measurement of the HU values between the original computational volume and the scanned physical breast model.

3. Results

3.1. Manufacturing of the physical breast phantom

Slices with segmented adipose, glandular, skin, and lesion tissues are shown in figure 5, in comparison to the original patient MRI slices. The first row (row I) in figure 5 shows the result of applying the segmentation procedure on a single MRI slice with three breast tissues (skin, adipose, glandular, no lesion present), while the second row (row II) shows the segmentation results for a single MRI slice with four breast tissues (skin, adipose, glandular, and lesion).

The final computational breast phantom is shown in figure 6(I-a), which computational phantom was printed in five separate parts with black PLA (figures 6(I-b), (I-c), (II)). The printing time was 7 days and the cost of the materials was estimated to approximately 30 euro.

3.2. Visual evaluation of the physical breast phantom

Figure 7 shows selected CT slices of the scanned physical breast phantom (figures 7(d)–(f)) in comparison to a slice taken from the computational breast phantom based on the segmented patient MRI breast volume (figure 7(a)) and segmented patient breast CT images from Sarno *et al* (figures 7(b), (c)), acquired at dedicated

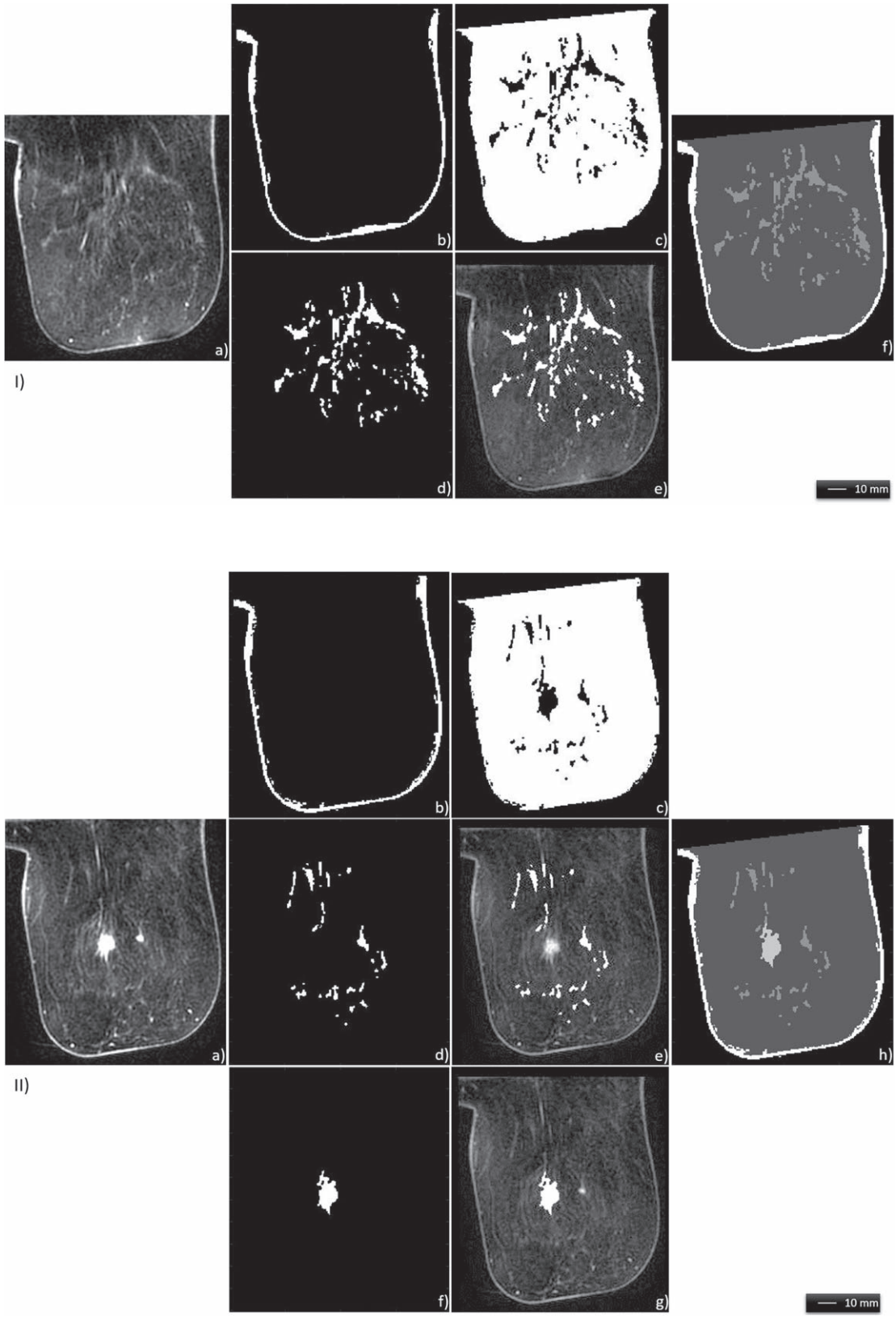

Figure 5. Results of the segmentation procedure. Row (I): (a) a slice from the patient MRI set, (b) segmented skin, (c) segmented adipose tissue, (d) segmented glandular tissue, (e) an overlay image of the segmented glandular tissue and the corresponding MRI slice, (f) a slice with the combined segmented tissues (skin, adipose and glandular). Row (II): (a) a slice from the patient MRI set, (b) segmented skin, (c) segmented adipose tissue, (d) segmented glandular tissue, (e) an overlay image of the segmented glandular tissue and the corresponding MRI slice), (f) segmented tumour, (g) an overlay image of the segmented tumour and the corresponding MRI slice (h) a slice with the combined segmented tissues (skin, adipose, glandular and tumour).

Figure 6. Final computational and printed models. (I-a) the computational breast model, (I-b), (I-c) the printed breast model, (II) the five separate parts comprising the breast printed model, and (III) a zoomed view of parts 3 and 4 with some of the anatomical structures visible.

breast CT facility (Sarno *et al* 2021). The images in figures 7(b), (c) are shown to demonstrate the visual similarity between the segmented set in this study and other publically available segmented breast sets.

The noticeable black lines on the images in figures 7(e), (f) are due to the fact that the phantom has been printed in 5 different parts and then assembled, which resulted in small air gaps in the final phantom assembly. The misalignment between the different parts of the printed breast are due to the double-sided adhesive tape used to bring the parts together and their displacement during the process of placing and scanning at the CT system.

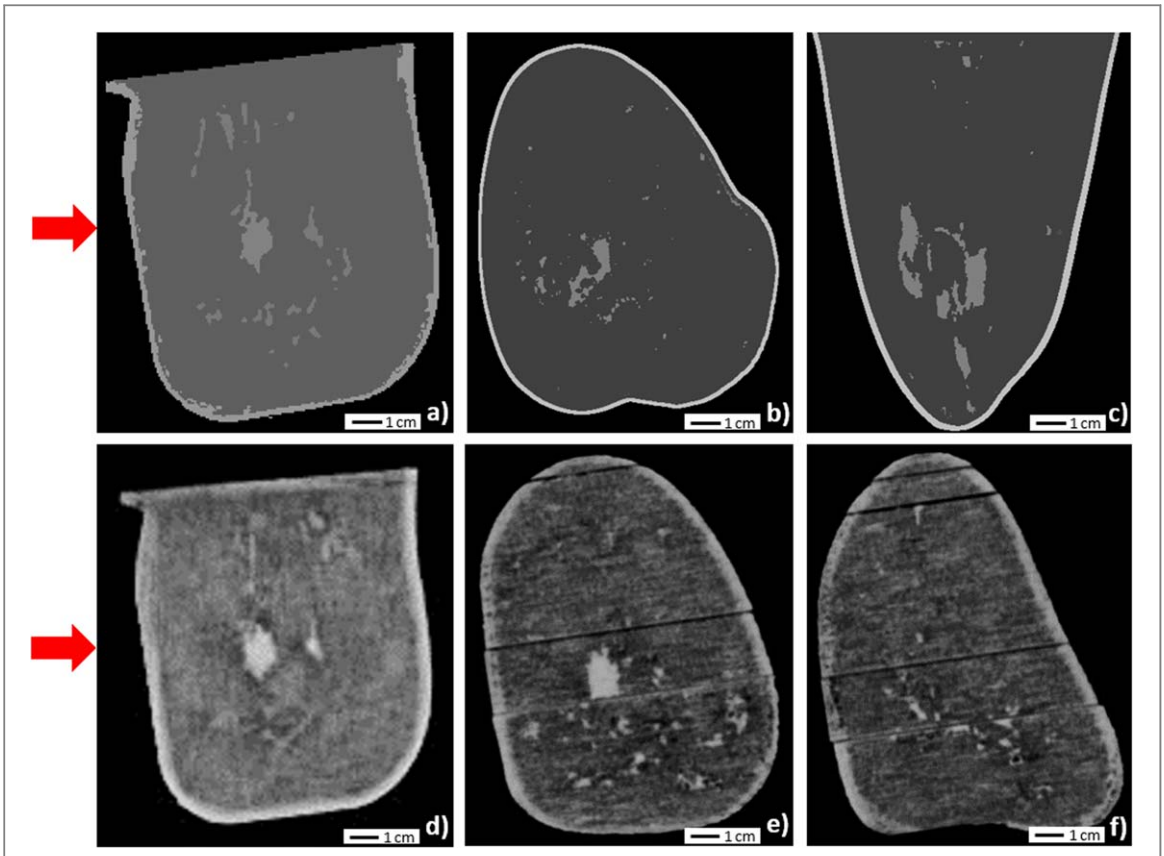

Figure 7. Visual assessment of the original computational and 3D printed breast phantoms: (a) a slice from the computational breast model (the red arrow indicates the position from which a line profile was taken), (b, c) axial and coronal slices from uncompressed computational breast phantom obtained from a real breast CT examination. Reproduced from Sarno *et al* 2021. CC BY 4.0. (d) a CT slice with lesion from the scanned physical breast model - coronal view (the red arrow indicates the position from a which line profile was taken), (e) a CT slice with lesion from the scanned physical breast model - axial view, (f) a CT slice without lesion from the scanned physical breast model - axial view.

Table 4. Summarized results of the subjective evaluation in percentages.

Questions	No	Rather No	Cannot decide	Rather Yes	Yes
Is there any lesion in the images?[a]	0%	0%	0%	33%	67%
Is there any lesion in the images?[b]	17%	33%	50%	0%	0%
Is the lesion realistic?	0%	0%	0%	44%	56%
Do you distinguish the individual breast tissues (glandular tissue, adipose tissue, lesions, and skin) from the model?	0%	0%	0%	60%	40%
Are the modelled breast components realistic?	0%	0%	0%	73%	27%
Is the breast model realistic as a whole?	0%	0%	0%	100%	0%

[a] The images are with lesions. Number of sets of images with lesions is 3.
[b] The images are without lesions. Number of sets of images without lesions is 2.

The visual assessment of the CT slices from the physical breast phantom, shown in figure 7, reveals a high degree of radiological similarity for the case of breast lesion. The skin and the glandular tissue structures are also well reproduced. This is well supported by the subjective evaluation, summarised in table 4.

3.3. Objective evaluation of the physical phantom

Line profiles are taken through the computational (figure 7(a)) and CT (figure 7(d)) slices and are shown in figure 8(a), demonstrating in general a good coincidence. The structures in the computational phantom are sharper due to the nature of the tissue characterisation of the computational model, while the edges of the structures in the printed phantom are smother due to the 3D printing and scattering x-ray effects, which occur at this energy of the x-rays.

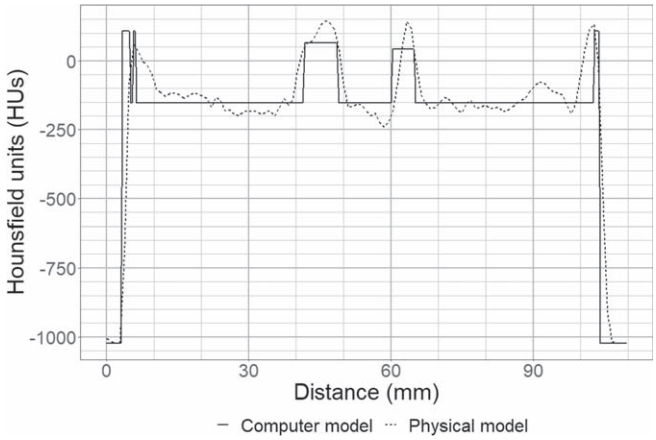

(a)

Printed tissue	Measured HU and SD	Percentage difference in respect to the computational phantom, %
Skin	110 ± 8	1.8
Adipose	-138 ± 8	10.1
Glandular	44 ± 3	4.5
Tumour	73 ± 25	12.3

(b)

Figure 8. A comparison of slices from the physical and the computational breast phantoms: (a) line profiles taken through the middle of a computational slice and a CT slice from the physical breast phantom (the position at which the profiles were taken is shown in figure 7(a) for the computational and figure 7(d) for the physical breast phantoms, with a red arrow), (b) measured HU values and standard deviations as well as a percentage difference of the physical breast phantom in respect to the computational one.

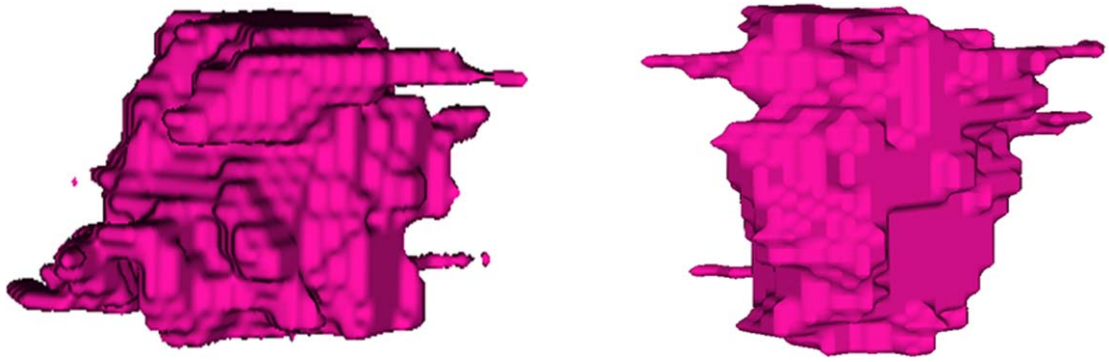

(a) (b)

Figure 9. Visualisation of the segmented tumours: (a) segmented from the original patient data, (b) segmented from the scanned physical breast model.

Further on, the measured HU values for the different breast tissues of the scanned breast phantom are summarised in figure 8(b). HU values and standard deviations were calculated after averaging the HU values for the studied tissues obtained from regions of interest in five consecutive slices with a lesion presence.

Another comparison includes the reproduction of the tumour volume. The original computational and the segmented lesion from the scanned physical breast model are visualised in figures 9(a), (b). The volume of the segmented tumour from the real patient MRI is 2091 mm^3, while the volume of the segmented tumour from the equivalent scanned breast model is 2016 mm^3. This translates into a relative error of 3.5%, which is an excellent result for the created breast model.

Further on, selected physical parameters were measured for both computational and physical breast models. Measurements were done for each physical part, shown in figure 6(II), as well as a whole. The results are summarised in table 5.

4. Discussion

This study used MRI patient data to produce both, computational and physical breast phantoms dedicated to x-ray imaging research. The goal of the segmentation procedure applied to distinguish the different breast tissue structures (skin, adipose, glandular, and tumour) was to obtain an accurate segmentation and correct representation of the different breast structures. The outcomes demonstrated a high degree of punctuality and clinical appearance, based on the radiologists' evaluation for image set 5 (which includes evaluation of the

Table 5. Comparison of physical parameters of the computational and physical breast phantoms.

Parameter		Part 1	Part 2	Part 3	Part 4	Part 5	Total
Height, mm	Computational	23.3	9.0	55.5	22.5	53.3	163.5
	Physical	22.7	9.9	55.3	22.6	53.4	163.9
Width, mm	Computational	100.6	101.8	106.6	111.4	112.0	112.0
	Physical	99.5	100.4	99.1	104.9	111.8	111.8
Length, mm	Computational	70.6	95.2	125.8	125.8	124.0	125.8
	Physical	68.6	95.3	125.5	125.5	123.5	125.5
Weight, g	Computational	42.6	38.1	460.9	236.6	417.7	1195.8
	Physical	35.6	41.3	457.3	232.6	415.0	1181.8

computational model) and the results in table 4. Visually, the segmented breast structures are also very similar to the segmented tissues that can be observed in the 150 digital breast models, recently reported by Sarno *et al* (Sarno *et al* 2021), an example of which is shown in figure 7(b), (c). These are obtained through segmenting patients' breast CT images, acquired with a dedicated breast CT facility (Sarno *et al* 2021). This similarity suggests that the exploited approach for creation of computational breast models based on MRI patient datasets can be used as an alternative to models derived from a breast CT.

Further, the subjective evaluation of CT slices of the physical breast phantom showed that the radiologists clearly distinguished the different printed breast tissues. The evaluation results (depicted in table 4), in view of radiological appearance, revealed that the different breast components and the breast model as a whole are realistically presented. The visual assessment of the CT slices, shown in figure 7, reveals a high degree of radiological similarity for the case of breast lesion. The skin and the glandular tissue structures are also well reproduced. This is well supported by the subjective evaluation, summarised in table 4. All three radiologists declared that they could observe the presence of a lesion on the CT slices, which actually contain a breast lesion. Moreover, all of them considered the lesion to have a realistic radiological appearance. All radiologists indicated that the shown lesion is malignant, which is the actual case. In case of image sets with no lesion, half of the radiologists' replies correctly reflected the real case (the absence of lesion in the images), while the other half were attributed to 'cannot decide' based on the provided image information. One of the radiologists' comments in this regard, if that was in a clinical situation she would ask for an additional examination from an ultrasound modality. These results confirm the realistic modelling of the computational breast lesion, implementation of the physical one, and the subjective radiological appearance of the breast lesion.

The measured HU values of the printed skin, glandular, and adipose structures (figure 8) are within the range of HU values (table 1) for the corresponding computational phantom structures. This demonstrates that the proposed approach for printing the normal breast structures correctly represents the corresponding radiological breast structures. The mean HU value and standard deviation of the printed tumour tissue is 73 ± 25, while the mean HU value of the computational tumour structure is 64. Overall, a good agreement between these values for the tumour structure is observed. The higher mean HU value for the printed tumour structure was due to the use of the perimetric pattern for the replication of the tumour tissue, resulting in an accumulation of small amounts of melted filament when the printing direction was radically changed. The segmented entities of the glandular tissue were smaller in size and simpler than the entity of the tumour tissue, and therefore they were less affected. The slice thickness of the scanned breast model was 3 mm, which explains the smooth edges of the tumour and other structures in the CT slices.

An excellent match between values of the physical parameters of the different parts of the printed and the computational breast phantoms is observed from the results in table 5. The whole physical breast phantom weights 1182 g, while the computational one weights 1196 g. The relative weight error is 1.2%, which is an excellent indicator for the printing technology and the proposed approach: using one PLA filament and different extrusion rates depending on the breast structure. Moreover, the relative errors in the linear dimensions between the computational and physical breast models were 0.24% (in length), 0.20% (in width), and 0.23% (in height), which is also a very good indicator for the correct representation of the four breast components by using PLA filament with an FDM technology. The spatial resolution of the phantom in x and y direction is affected by the diameter of the nozzle, which in this case is 0.4 mm, while in z direction, the resolution is affected by the layer height, which is 0.25 mm. By reducing these printing settings, the spatial resolution is expected to be further improved.

In a previous work, it was shown that it is possible to produce an anthropomorphic breast phantom using a series of patient CT images and a filament extrusion rate method (Daskalov *et al* 2020). This approach reduces considerably the number of the contoured entities, since only the area of interest is segmented, and can be implemented when CT scan images are utilized. However, it cannot be used when the data have been collected from other medical imaging systems such as an MRI scanner as used in this study. Hence, we proposed a

segmentation algorithm and a 3D printing process under a correlation of the MRI data with HUs for the 3D printing of anthropomorphic breast phantom. The MRI dataset provides an enhanced imaging of the soft tissues and improved tumour identification, resulting in 3D printed phantoms with realistically distributed and radiologically equivalent reproduced breast tissues. Since the 3D printing process of anthropomorphic phantoms is constantly being improved, results coming closer to human anatomy will be achieved. Future work will focus on the investigation of the combination of both 3D printing approaches employing data from a CT and an MRI scanners.

This study described the result of one patient's breast case, which is based on MRI images. Patients' images of breast MRI are continuously collected. The long-term goal of the international and interdisciplinary PHENOMENO project team is dedicated to collect patient breast images from both, breast CT and MRI exams within the four-year project period and to release a dedicated breast database (http://phenomeno.eu/). In practice, the creation of anthropomorphic breast phantoms is much related to the use of high-quality breast CT data, which is limited due to the low availability of such scanners worldwide. Although MRI is not the most appropriate choice for imaging the breast, due to the additional preparation work at a regular MRI system, this imaging modality turns out to be an alternative choice as a source of data for anthropomorphic breast models. Breast MRI has an advantage in cases of pre- and postoperative management of breast cancer. It is the most accurate way of determining the size of the cancer and whether there are other cancerous tissues in the same breast; also in assessing the residual disease after surgery. In contrary to CT, MRI does not involve radiation exposure and can therefore be safely used to screen women at increased risk of breast cancer.

Choosing breast MRI modality is also related to the development of thorough segmentation procedure, which will be subject to a comprehensive validation. In our current approach, breast MRI images are subjected to tissue segmentation in a breast volume, where the breast tissues are represented by HUs. The developed technique in this study is fully applicable to breast models obtained from breast CT images, and may be used with the dataset of 150 computational breast models reported by Sarno *et al* (Mettivier *et al* 2019, Sarno *et al* 2021), as a result of a classification algorithm applied on clinical breast CT images.

The produced anthropomorphic breast phantom is dedicated to x-ray imaging research and is planned for both, 2D and 3D breast imaging and dosimetry applications. The phantom is scheduled to be evaluated at a clinical tomosynthesis system: both tomosynthesis and mammography images as well as dose evaluation are planned. At the same time, the model will be evaluated at synchrotron facility, demonstrating the suitability of this technology for the creation of anthropomorphic phantoms for x-ray imaging research. For these evaluations, we will print the same phantom, however HUs will depend on the photon energy used. The quantity of the PLA in each voxel depends on the HU, which varies with the incident photon energies. In particular, the HU of the PLA increases with the increase of the photon energy. PLA is not frequently used as a material for mimicking the tissue attenuation at diagnostic x-ray energies due to its higher attenuation coefficients in respect to gland and adipose tissues (Ivanov *et al* 2018), rather it is used in phantoms dedicated to radiation therapy energies, (Dancewicz *et al* 2017). In order to use PLA for mimicking the radiological properties of the tissues, the voxel is printed with an extrusion rate which corresponds to a voxel infill less than 100%. The calibration procedure is implemented only once in case the incident x-ray spectra is known. The planned evaluations will also reveal the reproducibility of complex structures with the proposed method.

The evaluation of this phantom at a regular CT system showed that we need to improve further the printing method and use more appropriate printing materials, if we need to use the phantom for phase-contrast imaging applications. Further developments of the current printing technique concern improvement in the covering algorithm of the perimetric pattern to reduce the accumulated melted amounts of the filament, when there is a significant change of the printing direction. Other efforts are also focussed on the development of a printing method that can be used with higher density printing materials, which will overcome the 'air gaps' in the model. The possibility to obtain thinner and finer breast structures by printing smaller than 0.2 mm breast structures and using a narrower nozzle than 0.4 mm, which would result in an increased accuracy, will be also investigated. This would increase the printing time considerably, however, we plan to employ a couple of 3D printers working in parallel for producing different parts of the phantom, in order to reduce printing time.

5. Conclusions

This study demonstrated that a low-cost 3D printing system with a PLA filament can be used for manufacturing a physical anthropomorphic breast phantom, which phantom can provide realistic radiological images of the different breast tissues, when scanned. The study showed that the anatomical structures in both, the computational breast phantom slices and CT images of the physical breast phantom, exhibit a good degree of radiological similarity. This conclusion was well supported by the subjective evaluation, undertaken by three radiologists, as well as, by the objective quantitative evaluation, which included line profile comparison and

assessment of the physical and computational parameters of the corresponding phantoms. It can be concluded that the created physical anthropomorphic phantom satisfactory represents the characteristics and the spatial distribution of the different breast tissues, avoiding the need of using multiple printing materials with specific x-ray attenuation characteristics. The results of this study will be further exploited in the improvement of the proposed methodology and for development of a dedicated phantom for breast CT studies, and specifically in setting an experimental setup for an accurate breast CT dosimetry study. The data for this study is available at Zenodo repository (https://doi.org/10.5281/zenodo.5887359).

Acknowledgments

This work is supported by PHENOMENO action. This project has received funding from the European Union's Horizon 2020 research and innovation programme under the Marie Skłodowska-Curie grant agreement No 101008020.

ORCID iDs

Nikolay Dukov https://orcid.org/0000-0003-2697-6194
Kristina Bliznakova https://orcid.org/0000-0002-3630-5936
Zhivko Bliznakov https://orcid.org/0000-0003-0831-2511

References

Badal A, Clark M and Ghammraoui B 2018 Reproducing two-dimensional mammograms with three-dimensional printed phantoms *J Med Imaging (Bellingham)* **5** 033501

Berger M J, Hubbell J H, Seltzer S M, Chang J, Coursey J S, Sukumar R, Zucker D S and Olsen K 2010 *XCOM: Photon Cross section Database (version 1.5)* [Online] Available: (http://physics.nist.gov/xcom [Saturday, 26-Jul-2014 05:42:53 EDT]) (Gaithersburg, MD.: National Institute of Standards and Technology)

Bliznakova K *et al* 2019 Development of breast lesions models database *Phys. Med.* **64** 293–303

Bliznakova K 2020 The advent of anthropomorphic three-dimensional breast phantoms for x-ray imaging *Phys Med* **79** 145–61

Bliznakova K, Bliznakov Z, Bravou V, Kolitsi Z and Pallikarakis N 2003 A three-dimensional breast software phantom for mammography simulation *Phys. Med. Biol.* **48** 3699–719

Bliznakova K, Bliznakov Z and Pallikarakis N 2010 An improved algorithm for out-of-plane artifacts removal in digital tomosynthesis reconstructions *Published (Chalkidiki, 2010) (12th Mediterranean Conf. on Medical and Biological Engineering and Computing, MEDICON 2010, vol. Series 29) pp 367–370* (*IFMBE Proceedings* 29) *(Chalkidiki, Greece)* (Springer, Berlin, Heidelberg) (https://doi.org/10.1007/978-3-642-13039-7_92)

Carton A K, Bakic P, Ullberg C, Derand H and Maidment A D 2011 Development of a physical 3D anthropomorphic breast phantom *Med. Phys.* **38** 891–6

Dancewicz O L, Sylvander S R, Markwell T S, Crowe S B and Trapp J V 2017 Radiological properties of 3D printed materials in kilovoltage and megavoltage photon beams *Phys Med* **38** 111–8

Daskalov S, Okkalidis N, Boone J M, Marinov S, Bliznakov Z, Mettivier G, Bosmans H, Russo P and Bliznakova K 2020 Anthropomorphic physical breast phantom based on patient breast CT data *15th Mediterranean Conf on Medical and Biological Engineering and Computing, MEDICON 2019 (Coimbra, Portugal, 26–28 September, 2019)* pp 367–74

Dukov N, Bliznakova K, Feradov F, Buliev I, Bosmans H, Mettivier G, Russo P, Cockmartin L and Bliznakov Z 2019 Models of breast lesions based on three-dimensional x-ray breast images *Phys Med* **57** 80–7

Dukov N, Bliznakova K, Teneva T, Marinov S, Bakic P, Bosmans H and Bliznakov Z 2021 Experimental evaluation of physical breast phantoms for 2D and 3D breast x-ray imaging techniques *Published 8th European Medical and Biological Engineering Conf. (Portorož, 2021), vol. Series 80: Int. Publishing* (Springer: Berlin) pp 544–52

Elangovan P, Mackenzie A, Dance D R, Young K C and Wells K 2018 Lesion detectability in 2D-mammography and digital breast tomosynthesis using different targets and observers *Phys. Med. Biol.* **63** 095014

Di Franco F, Mettivier G, Sarno A, Varallo A and Russo P 2019 Manufacturing of physical breast phantoms with 3D printing technology for x-ray breast imaging *2019 IEEE Nuclear Science Symposium and Medical Imaging Conference (NSS/MIC) (Manchester, UK, 26 October–2 November 2019)* (Picastaway, NJ: IEEE) pp 1–5

Glick S J and Ikejimba L C 2018 Advances in digital and physical anthropomorphic breast phantoms for x-ray imaging *Med. Phys.* **45** E870–85

Ikejimba L C, Yan T, Kemp K, Salad J, Graff C G, Ghammraoui B, Lo J Y and Glick S J 2018 Methodology for the objective assessment of lesion detection performance with breast tomosynthesis and digital mammography using a physical anthropomorphic phantom *Medical Imaging 2018: Physics of Medical Imaging* **10573**

Ivanov D *et al* 2018 Suitability of low density materials for 3D printing of physical breast phantoms *Phys. Med. Biol.* **63** 175020

Kiarashi N, Nolte A C, Sturgeon G M, Segars W P, Ghate S V, Nolte L W, Samei E and Lo J Y 2015 Development of realistic physical breast phantoms matched to virtual breast phantoms based on human subject data *Med. Phys.* **42** 4116–26

Malliori A, Bliznakova K, Sechopoulos I, Kamarianakis Z, Fei B and Pallikarakis N 2014 Breast tomosynthesis with monochromatic beams: a feasibility study using Monte Carlo simulations *Phys. Med. Biol.* **59** 4681–96

Malliori A, Bliznakova K, Speller R D, Horrocks J A, Rigon L, Tromba G and Pallikarakis N 2012 Image quality evaluation of breast tomosynthesis with synchrotron radiation *Med. Phys.* **39** 5621–34

Mettivier G, Bliznakova K, Sarno A, Lillo F D, Castriconi R and Russo P 2017 In-line phase contrast tomography of the breast with a dedicated micro-CT scanner *IEEE Nuclear Science Symp., Medical Imaging Conf. and Room-Temperature Semiconductor Detector Workshop, NSS/MIC/RTSD 2016,2017) (Strasbourg, France, 29 October–6 November 2016)* (Picastaway, NJ: IEEE) pp 1–3

Mettivier G, Sarno A, Franco F D, Bliznakova K, Bliznakov Z, Hernandez A M, Boone J M and Russo P 2019 The Napoli-Varna-Davis project for virtual clinical trials in x-ray breast imaging *Published 2019 IEEE Nuclear Science Symp. and Medical Imaging Conf., NSS/MIC 2019,2019), vol. Series): Institute of Electrical and Electronics Engineers Inc.) (Manchester, UK, 26 October–2 November 2019)* (Picastaway, NJ: IEEE) pp 1–5

Okkalidis N 2018 A novel 3D printing method for accurate anatomy replication in patient-specific phantoms *Med. Phys.* **45** 4600–6

Okkalidis N and Marinakis G 2020 Technical note: accurate replication of soft and bone tissues with 3D printing *Med. Phys.* **47** 2206–11

Santos J C, Almeida C D, Iwahara A and Peixoto J E 2019 Characterization and applicability of low-density materials for making 3D physical anthropomorphic breast phantoms *Radiat Phys Chem* **164** 1-8

Sarno A, Mettivier G, di Franco F, Varallo A, Bliznakova K, Hernandez A M, Boone J M and Russo P 2021 Dataset of patient-derived digital breast phantoms for in silico studies in breast computed tomography, digital breast tomosynthesis, and digital mammography *Med. Phys.* **48** 1–12

Schopphoven S, Cavael P, Bock K, Fiebich M and Mäder U 2019 Breast phantoms for 2D digital mammography with realistic anatomical structures and attenuation characteristics based on clinical images using 3D printing *Phys. Med. Biol.* **64** 215005

Sikaria D, Musinksy S, Sturgeon G, Solomon J, Diao A, Gehm M, Samei E, Glick S and Lo J 2016 Second generation anthropomorphic physical phantom for mammography and DBT: Incorporating voxelized 3D printing and inkjet printing of iodinated lesion inserts *Proc. SPIE* **9783** 978360

Tino R, Yeo A, Leary M, Brandt M and Kron T 2019 A systematic review on 3D-printed imaging and dosimetry phantoms in radiation therapy *Technol Cancer Res T* **18** 1533033819870208

Zhao C, Solomon J, Sturgeon G M, Gehm M E, Catenacci M, Wiley B J, Samei E and Lo J Y 2017 Third generation anthropomorphic physical phantom for mammography and DBT: incorporating voxelized 3D printing and uniform chest wall QC region *Proc SPIE* **10132** 101321Y